Journal of Power Sources 195 (2010) 2196–2201

Contents lists available at ScienceDirect

Journal of Power Sources

journal homepage: www.elsevier.com/locate/jpowsour

Synthesis and electrical properties of apatite-type $La_{10}Si_6O_{27}$

Bin Li*, Wei Liu, Wei Pan*

State Key Lab. of New Ceramics and Fine Processing, Department of Materials Science and Engineering, Tsinghua University, Beijing, 100084, People's Republic of China

ARTICLE INFO

Article history:
Received 21 July 2009
Received in revised form 22 October 2009
Accepted 27 October 2009
Available online 6 November 2009

Keywords:
Oxy-apatite
Co-precipitation
Nanopowders
Electrical conductivity
Solid oxide electrolyte

ABSTRACT

Lanthanum silicate $La_{10}Si_6O_{27}$ nanopowders are synthesized via co-precipitation process. After the calcination at 900 °C and then removal of La_2O_3 by acid-washing, pure stoichiometric $La_{10}Si_6O_{27}$ nanopowders are obtained, and are characterized by XRD, BET, TEM and ICP, respectively. The oxy-apatite ceramic with the density higher than 95% can be obtained at rather low sintering temperature of 1300 °C, which has comparable total conductivity with the samples sintered at 1650 °C from the powders prepared by solid-state reaction. Additionally, effects of sintering temperatures on electrical properties are also investigated in detail. It is found, that with the increasing sintering temperature from 1300 °C to 1650 °C, the grain conductivity monotonously increases; while the grain boundary conductivity increases first and then decreases with the maximum value at 1600 °C. The related mechanism is also discussed.

1. Introduction

With their ability to directly and efficiently convert chemical energy to electrical energy without pollution, fuel cells have been intensively studied for application as energy conversion devices. Among these fuel cells, the solid oxide fuel cell (SOFC) has been recognized as a favorable system for stationary and auxiliary power units. Currently, yttria-stabilized zirconia (YSZ) is the most common material used as electrolyte for SOFC due to its very excellent ionic conductivity negligible electric conduction over a wide range of $p(O_2)$, and good chemical stability [1–3]. Nevertheless, the operating temperature is too high (>800 °C), which will result in some troubles, such as the degradation of its constituent components, undesirable interfacial reaction in between, and the choice of interconnectors and seals. To overcome these problems, one of the approaches is to develop new solid electrolyte materials, which have higher ionic conductivity being more profitable for lower temperature application. Ceria based [1–3] and $LaGaO_3$ based [1–3] electrolytes have been extensively investigated during these years. Both these systems have higher oxide-ion conductivities than YSZ, although they have their problems particularly under the reducing conditions of the SOFC anode, where electronic conduction can be introduced in the case of ceria based electrolytes, while Ga volatility can occur in terms of the gallate.

Recently, rare earth silicates having apatite-type structure in the general formula $RE_{9.33+x}Si_6O_{26+1.5x}$ (RE, rare earth elements) are a new class of oxide-ion conductors first found by Nakayama et al. [4,5]. Because of low activation energy and especially excellent stability over a wide oxygen partial pressure range [6,7], the compounds seem to be potential candidates for IT-SOFC electrolytes. Most studies have been focused on the lanthanum silicate-based apatites which show higher oxide-ion conductivity than other rare earth apatites [5]. As is well known, in materials with fluorite (e.g. doped ZrO_2, CeO_2) or perovskite (e.g. doped $LaGaO_3$) related structures, conduction progresses via oxide ion vacancies [1–3]. However, in the apatite silicates oxygen ions are confirmed to migrate via an interstitial conduction mechanism; excess oxide ions can be introduced in the structure and facilitate oxide-ion migration in the conduction channel by a complex sinusoidal pathway along the *c*-axis [8,9]. The conductivity is enhanced with increasing the La composition from 9.33 to 10, which is ascribed to introduction of excess oxide ions from the stoichiometric oxygen composition of 26. Nevertheless, the main limitation of such materials resides in the difficulty to prepare pure and dense ceramics. The traditional method explored for preparing this material is solid-state reaction, which has encountered some troubles. For example, especially for $La_{10}Si_6O_{27}$, there is often impurity such as La_2SiO_5, which tends to degrade the electrical performances of the entire electrolyte [8,10]. Additionally, from powders synthesized by solid-state reaction, very high sintering temperatures (1650 °C or 1700 °C) even preceded by specific treatments (intermittent ball-milling), are still necessary to obtain relative densities higher than 90%, which may result in increasing of the energy exhaust, and hindering the co-firing of electrolytes with other SOFCs ele-

* Corresponding authors. Tel.: +86 10 62772858; fax: +86 10 62771160.
E-mail addresses: bli05@mails.tsinghua.edu.cn (B. Li), panw@mail.tsinghua.edu.cn (W. Pan).

0378-7753/$ – see front matter.
doi:10.1016/j.jpowsour.2009.10.088

ments [11,12]. Accordingly, lower synthesis temperatures allow dispersed/nanocrystalline powders to be obtained, which play a crucial role in the sintering and densification of oxides. Some low-temperature preparation methods such as sol–gel route [13–15], freeze-drying [16,17], and mechanochemical milling [18,19] have been used, but it is still very difficult to obtain pure powders or dense bulks. For instance, for sol–gel methods, as reported by Tao et al., the methods lead only to relative densities smaller than 80% even after sintering of 1400 °C during 3 days or 1500 °C during 22 h [14]. Recently, Tian et al. [15] reported a better result with a density of 92% after 1550 °C for 10 h, but after sintering of 1400 °C, the density is still low (73%).

In the present work, the nanopowders are synthesized via simple co-precipitation process, and the influence of sintering temperature on transport properties is investigated. Previous studies found the conductivity increased with increasing the sintering temperature, which is mainly related to the enhancement of density [4,5]. In our work, the high density (>95%) can be obtained under lower sintering temperature, the trends about conductivity with sintering temperature are perhaps different.

2. Experimental

Precursor powders were produced via co-precipitation using ammonium hydroxide as precipitant. The starting salts are $La(NO_3)_3{\cdot}6H_2O$ and tetraethyl orthosilicate (TEOS). The stock solution of starting salts was made by dissolving stoichiometric $La(NO_3)_3{\cdot}6H_2O$ and TEOS in proper distilled water and ethanol. The volume ratio of water and ethanol is fixed to be 1:4. No turbidity and precipitate was observed at this stage. The final concentration of the resulting clear transparent solution was 0.4 M for La^{3+}. Then the solution was dropped into dilute ammonia (pH 9) solution under vigorous stirring and ultrasonic oscillation to form a white gel at room temperature. The gels were then collected by vacuum filtration, washed three times with water and three times with alcohol, and then dried at 100 °C for 12 h. The dried precursor was then calcined at 800 °C, 900 °C, 1000 °C and 1100 °C for 6 h, respectively. For comparison, the powders were also synthesized by conventional solid-state reaction, according to the process mentioned by Yoshioka [11] and Shaula et al. [12].

Simultaneous TG/DSC (STA409PC, Netzsch, Germany) experiments were performed on part of the dried gel precursors in order to study the synthesis process. Temperature ranges of analysis were from room temperature to 1200 °C with a heating rate of 5 °C min^{-1} in a flowing air atmosphere. Phase identification and analysis were conducted using X-ray diffraction (XRD). Two kinds of XRD scans were performed using an X-ray diffractometer (Rigaku, D/max-RB, Japan) with nickel-filtered Cu Kα radiation. Continuous scans (8° min^{-1}) were used for qualitative phase identification, while slow step scans at a rate of 0.02°/2 s were conducted to estimate the grain sizes (D_{XRD}) and the lattice parameters. Grain sizes of the as-calcined powders were calculated by the X-ray line broadening technique performed on the (5 0 2) diffraction of $La_{10}Si_6O_{27}$ lattice from the Scherrer equation. Lattice parameters of the specimens were calculated from slow step scan XRD data, using the least-squares method. The specific surface area (S_{BET}, m^2 g^{-1}) of the as-synthesized powders was measured by the standard Brunauer–Emment–Teller (BET) technique with N_2 adsorption (NOVA4000, America). The specific surface area was converted into average particle size (D_{BET}, nm) according to the following equation assuming that the particles are closed spheres with smooth surface and uniform size:

$$D_{BET} = \frac{6000}{S_{BET} \cdot \rho_{th}} \quad (1)$$

where ρ_{th} (g cm^{-3}) is the theoretical density of the material, which can be calculated from the values of lattice parameters. The ρ_{th} values can be estimated according to:

$$\rho_{th} = \frac{10M_{La} + 6M_{Si} + 27M_O}{N_A \cdot \sqrt{3}/2 \cdot a^2 c} \quad (2)$$

where a and c are the lattice constants, N_A is the Avogadro constant, and M_i refers to the atomic weight. Particle sizes (D_{TEM}), morphology and agglomeration state of the as-synthesized powders were observed via high-resolution transmission electron microscope (HRTEM, JEM-2011, Japan). The real composition (La/Si) was tested by inductively coupled plasma mass spectroscopy (ICP, X Series). The as-synthesized powders were sieved to 200 meshes, isostatic cool pressed under 200 MPa, and then sintered at 1300 °C, 1400 °C, 1500 °C, 1600 °C and 1650 °C for 10 h, respectively. All the specimens were sintered in air and heated by the rate of 4 °C min^{-1}, and then furnace-cooled after sintering. Densities of the sintered pellets were determined by Archimedean method. The sintered pellets were polished, thermally etched, and gold coated for microstructural analysis using scanning electron microscopy (SEM, SSX-550, Japan). The average grain sizes were obtained from SEM micrographs of the etched samples by using the linear intercept technique described by Mendelson [20]. The grain and grain boundary conductivities in air were determined by ac impedance spectroscopy (Zenar, IM6, German). Silver electrodes were coated on both surfaces of the sintered pellets and heated at 550 °C for 30 min. Impedance measurement was performed on heating from 250 °C to 700 °C in a frequency range from 0.1 Hz to 8 MHz with an increment of 50 °C, and followed by analyzing these results using Z-View software.

3. Results and discussion

Fig. 1 shows the TG/DSC curves of dried precursor heated from room temperature to 1200 °C at 5 °C min^{-1} in air. It can be seen that an important weight loss (~25%) occurs in several steps between RT and 600 °C. Simultaneously, the DSC plot shows a wide exothermic peak from 150 °C to 350 °C, indicating several chemical reactions over this temperature range. That is presumably related with the formation of oxy-apatite phase. Above 600 °C, the TG curve turns flat, but there is an exothermic peak among 830–880 °C for DSC plot. Corresponding to the curve of TG/DSC, the dried precursors are calcined at 800 °C and 900 °C, respectively, without holding time. It can be seen form Fig. 2 that the XRD patterns of the powders reflect the amorphous natures for 800 °C and crystalline natures for 900 °C without holding time. So the exothermic peak can be considered to

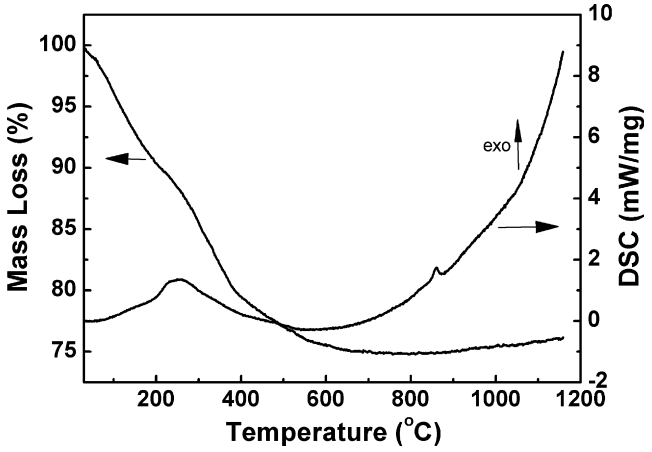

Fig. 1. TG/DSC curves of dried precursor heated from room temperature to 1200 °C at 5 °C min^{-1} in air.

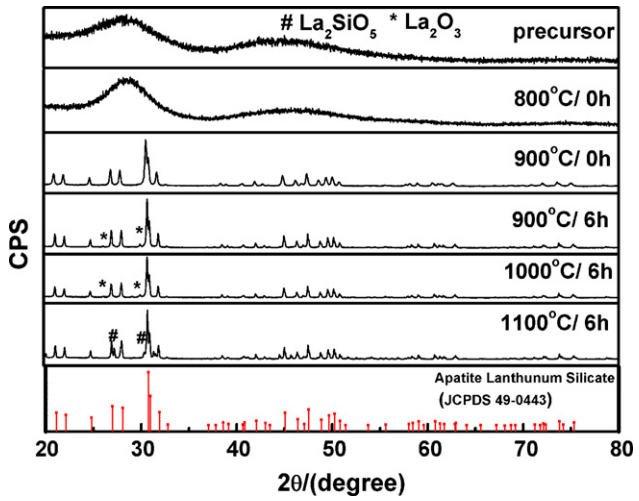

Fig. 2. XRD patterns of the precursors and the powders calcined at 800 °C/0 h, 900 °C/0 h, 900 °C/6 h, 1000 °C/0 h, and 1100 °C/6 h.

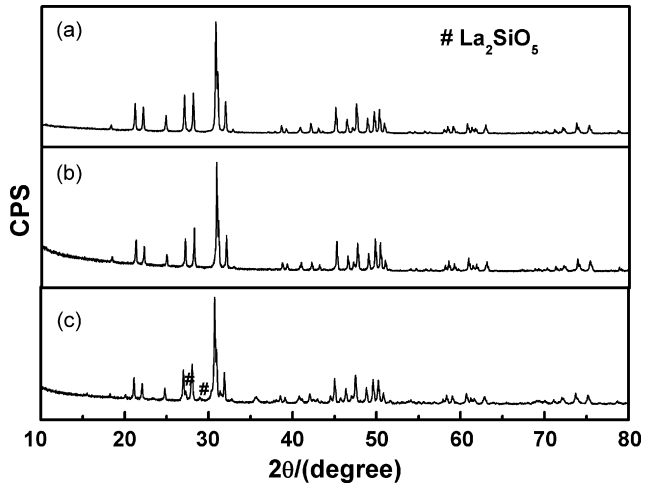

Fig. 3. XRD patterns of the $La_{10}Si_6O_{27}$ powders calcined at 900 °C for 6 h after acid-washing (a); and the corresponding bulks sintered at 1650 °C (b); and the bulks sintered at 1650 °C from the powders prepared by solid-state reaction (c).

be associated with the phase transition from amorphous to crystallized phase. Therefore, the oxy-apatite phase (amorphous) can be formed at lower temperature (below 600 °C), and the integrated chemical reaction is shown as follows:

$$La(OH)_3 + SiO_2 \rightarrow \text{ apatite} \quad (3)$$

And it can be well crystallized above about 900 °C for the above-mentioned method. In the process of conventional solid-state reaction, the typical synthesis temperature for oxy-apatites is 1300 °C [4,5,8,11,12], which is much higher than that by co-precipitation.

XRD patterns of powders calcined at 900 °C, 1000 °C and 1100 °C for 6 h are also displayed in Fig. 2. Only oxy-apatite phase is observed for the powder calcined at 900 °C without holding time according to the JCPDS 49-0443 in Fig. 2, but the impurity of La_2O_3 phase occurs when extending the holding time to 6 h, which can be explained that a secondary amorphous phase (La_2O_3) exists at 900 °C, and crystallizes for longer time. La_2O_3 phases remain unchanged up to 1000 °C. Nevertheless, at 1100 °C, another phase (La_2SiO_5) occurs accompanied by the disappearance of La_2O_3 phases. As is known, the La_2SiO_5 phases are easily formed while the oxy-apatite phases are synthesized with the solid-state reaction method [8,10]. However, for the co-precipitation method, the above phenomenon displays that the formation temperature of La_2SiO_5 is higher than that of oxy-apatite phase, and the presence of La_2O_3 at lower temperature leads to the formation of La_2SiO_5 phase at higher temperature, which can be described as

$$La_2O_3 + La_{10}Si_6O_{27} \rightarrow 6La_2SiO_5 \quad (4)$$

Accordingly, in order to obtain the pure oxy-apatite phase, the La_2O_3 phase must be removed at lower temperature. Before the purification, the dried precursors are calcined at 900 °C for 6 h to obtain well-crystallized materials, and at this calcination temperature, only La_2O_3 phase, besides oxy-apatite phase, is observed (Fig. 2). By adding dilute HNO_3 solution and controlling pH ≈ 4, the resultant powders are acid washed. Fig. 3(a and b) shows XRD patterns of the powders after acid-washing and the corresponding bulk sintered at 1650 °C for 10 h. No other phases besides oxy-apatite phase are found, which can further be an evidence for the mentioned chemical reaction (4).

The TEM image, displayed in Fig. 4, illustrates the morphology and internal crystal structure of individual nanoparticles for the $La_{10}Si_6O_{27}$ powders prepared by calcination of the precursor at 900 °C for 6 h after acid-washing. The sizes of spherical nanoparticles are found to occupy a narrow size range. The mean particle size is around 40 nm. The average grain size estimated from the XRD data using Scherrer equation is approximately 42 nm. And the average particle size calculated from the BET data assuming that the particles are closed spheres with smooth surface and uniform size is about 51 nm. The two values (presented in Table 1) show excellent agreement, which indirectly confirms the powders are not strongly agglomerated. And the direct evidence is that individual nanoparticles viewed in HRTEM images appear to be single crystals, as displayed in inset (a) of Fig. 4, to exhibit high crystallinity and to have essentially non-defective structures, despite their very small dimensions and relatively low synthesis temperature. As shown in inset (b) of Fig. 4, Digital Diffraction Patterns (DDPs) are calculated by performing a mathematical Fourier transfer on inset (a). It is indexed to apatite structure viewed in the $[\bar{1}\,\bar{2}\,4]$ zone axes. Compared with other low temperature synthesis methods, such as

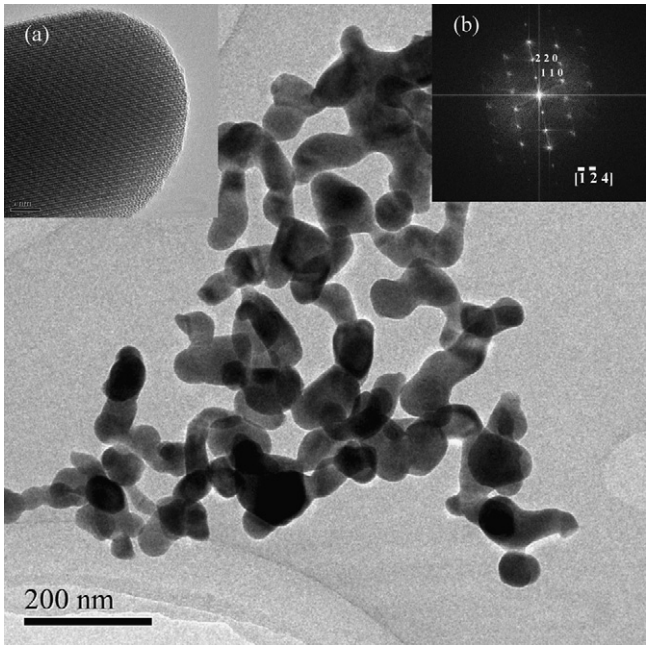

Fig. 4. The TEM image of the $La_{10}Si_6O_{27}$ powder prepared by calcination of the precursor at 900 °C for 6 h after acid-washing. Inset (a) and (b) are the HRTEM image and corresponding Fourier transformation.

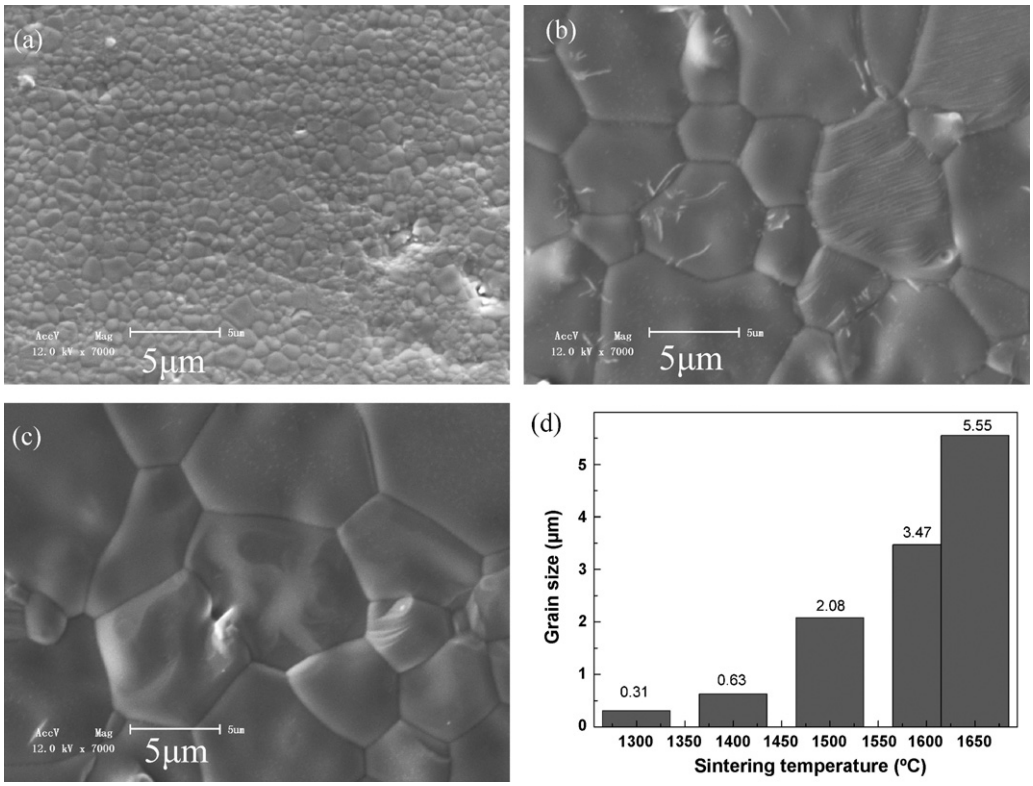

Fig. 5. SEM micrographs of $La_{10}Si_6O_{27}$ sintered at 1400 °C (a) and 1650 °C (b and c) for 10 h ((a and b) co-precipitation; (c) solid-state reaction); average grain size of the bulks versus sintering temperature (d).

sol–gel reported by other investigators [13–15], particles prepared in our case are weakly agglomerated, which is perhaps attributed to the use of ultrasonic oscillation during preparation of precursors.

Because of the final process of acid-washing, the actual composition needs to be tested again. By the measurement of ICP, the mole ratio of La/Si is 10.1/6 (listed in Table 1), which is very close to the ideal value 10/6. The stoichiometric nanopowders can be considered to be successfully synthesized. The lattice parameters can be calculated by XRD values, which are also listed in Table 1. So the theoretical density can be estimated to be 5.62 g cm^{-3} by Eq. (2).

In order to satisfy the application for SOFC, the relative density of the electrolyte is at least equal to 95%. In our work, the samples were sintered at 1300 °C, 1400 °C, 1500 °C, 1600 °C and 1650 °C for 10 h, respectively. The actual densities of all the sintered pellets are measured by Archimedean method. We observe that the relative densities of all the samples are higher than 95%, which are consistent with the results of SEM, as shown in Fig. 5(a–c). And Fig. 5(d) shows the average grain size varies from 0.31 μm to 5.55 μm with increasing sintering temperature from 1300 °C to 1650 °C. For conventional solid-state reaction methods, the densification temperature is up to 1650 °C or 1700 °C [4,5,11,12]. The use of lower temperatures such as 1500 °C during 16 h leads to poorly densified samples with relative density lower than 70% [21]. Even the use of soft chemistry hardly leads to totally convincing results, such as sol–gel methods [14,15], because the dispersity of nanopowders is weak, leading to high sintering temperature. In our work, as seen in Fig. 4, the nanopowders are not strongly agglomerated, corresponding to the largely reduced sintering temperature (1300 °C). The resulting high relative density ensures negligible porosity effects on the electrical conductivity reported in this work.

Ac impedance measurements were conducted on the series of $La_{10}Si_6O_{27}$ in the temperature range of 250–700 °C in air. In a typical AC impedance measurement, the complex impedance of a sample as a function of frequency is measured. Generally, in polycrystalline specimens, two independent semicircular arcs from high frequency to low frequency correspond to the conduction across the grains (R_g) and grain boundaries (R_{gb}), and a diffusion-limited process leads to an impedance response (Warburg impedance Z_w) that appears as a straight line in the lower frequency range, as shown in Fig. 6(a–e). The corresponding equivalent circuit is displayed in Fig. 6(f), which is applied to fit the experimental data, and then the corresponding R_g and R_{gb} are calculated. In the present case, in place of a capacitor, a constant phase element (CPE) is used to fit the experimental data accounting for the microstructure inhomogeneity within the specimen. In general, each individual resistance (shown in Fig. 5), R_i, can be formally converted to a conductivity σ_i, using the equation:

$$\sigma_i = \frac{l}{R_i S} \tag{5}$$

where l is the sample thickness and S is the electrode area of the sample surface. In this way, the total conductivity (σ_{total}), the grain conductivity (σ_g), and the apparent grain boundary conductivity (σ_{gb}) can be obtained.

Table 1
Real composition, lattice parameters, D_{XRD} and D_{BET} of the powders of $La_{10}Si_6O_{27}$ calcined at 900 °C for 6 h after acid-washing.

Composition	Real composition	Lattice parameter (apatite)		D_{XRD} (nm)	D_{BET} (nm)
	La/Si	a (Å)	c (Å)		
$La_{10}Si_6O_{27}$	10.1/6	9.721	7.186	42	51

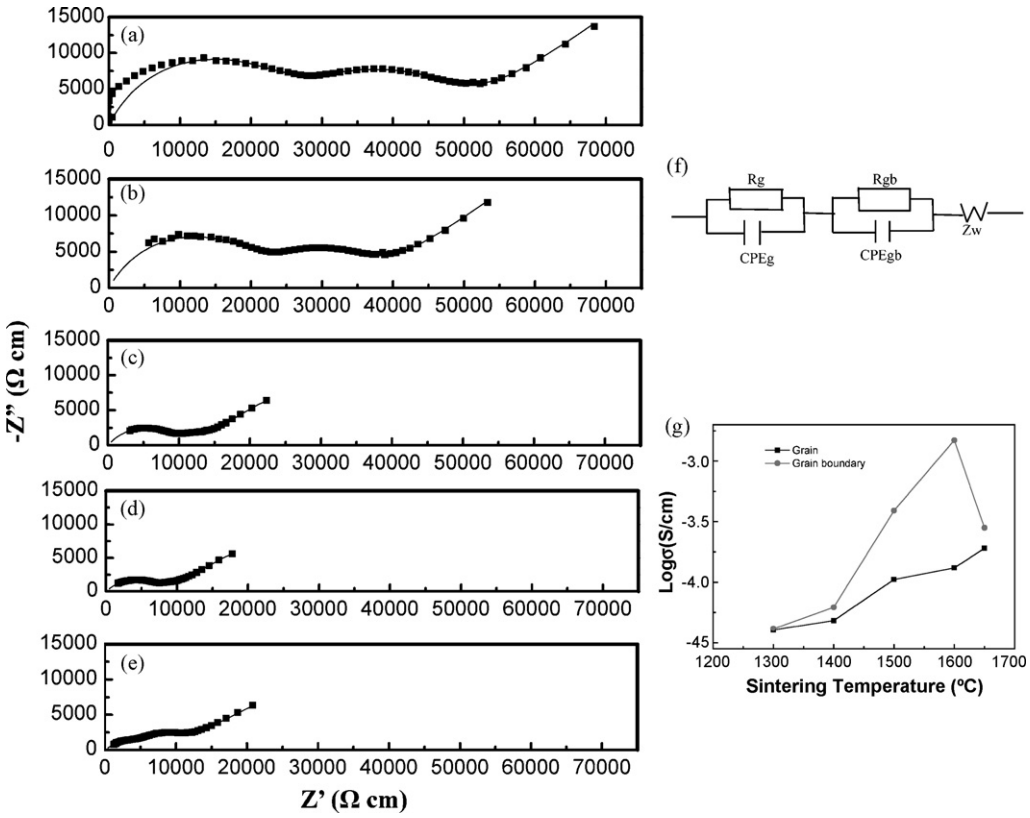

Fig. 6. The ac impedance spectra and fitted lines of $La_{10}Si_6O_{27}$ sintered at 1300 °C (a), 1400 °C (b), 1500 °C (c), 1600 °C (d) and 1650 °C (e) for 10 h measured at 400 °C; corresponding schematic equivalent circuits (f); grain and grain boundary conductivities of the samples measured at 400 °C versus sintering temperature (g).

As shown in Fig. 6(g), for the samples measured at 400 °C, with the increasing sintering temperature, the grain conductivity monotonously increases; while the grain boundary conductivity increases first and then decreases with the maximum value at 1600 °C.

At low measuring temperatures, the ac impedance spectroscopy plots exhibit clear grain and grain boundary arcs (Fig. 6(a–e)). As the measuring temperature is increased, the time constants of the relaxations resulting from the individual polarizations are reduced and hence the arcs are shifted to higher frequencies. This results in the successive disappearance of the arcs corresponding to the grain and grain boundary contributions. And finally only the electrode contribution is seen at higher measuring temperatures. In our work, the contribution from the grain boundary process cannot be observed above 500 °C. Hence, the grain and grain boundary conductivity are shown in Fig. 7(a and b) below 500 °C. For the sample sintered at 1600 °C, the grain boundary conductivity is not shown, due to too small arc corresponding to grain boundary conduction at some measuring temperature. The trends about σ_g and σ_{gb} with sintering temperature measured below 500 °C are consistent with that at 400 °C. The enhancement of grain conductivity with increasing temperature is perhaps attributed to the homogeneousness of the composition. As mentioned in the introduction, the series of $La_{9.33+x}Si_6O_{26+1.5x}$ $(0 \le x \le 0.67)$ exhibit the oxy-apatite phase, and the conductivity improves with the increase of x. Higher sintering temperature promotes solid diffusion, leading to more homogeneous $La_{10}Si_6O_{27}$ composition formed. In addition, the maximum value at some sintering temperature suggests that two antagonist effects on the grain boundary conductivity were shown with the increase of sintering temperature. On the one hand, the reduction of grain boundaries results in the improvement of apparent grain boundary conductivity. On the other hand, higher sintering temperature perhaps promotes the segregation of La^{3+} to the grain boundaries. In the crystal structure of oxy-apatite lanthanum silicate, La^{3+} takes up two positions: 4f and 6h [8–10]. The stable existence of the cation vacancy at the position of 4f [11] suggests that La^{3+} could thermally diffuse easily. Therefore, the accumulation of La^{3+} at the grain boundaries inhibits the conduction of oxide ions, which needs to be further studied by TEM. Owing to the antagonist influencing factors, the appropriate sintering temperature (1600 °C) with the maximum conductivity value presents, as shown in Figs. 6(c) and 7(b). Fig. 7(c) shows the total conductivity of the samples sintered at different temperatures. Combining grain results with grain boundary results, it can be seen that the trend about σ_{total} with the sintering temperature is different in different measuring temperature ranges. In the low measuring temperature range (≤400 °C), the variety of grain boundary conduction plays an important role in that of total conduction. So the total conductivity increases with increasing the sintering temperature, and reaches the maximum value at 1600 °C, and then decreases. However, in the high measuring temperature range (>400 °C), the grain boundary has less effect on the total conductivity, so the total conductivity straightly improves with increasing sintering temperature, which is in agreement with the trend of grain conduction. The corresponding total activation energies of all the samples are all calculated according to slopes of the plots in Fig. 7(c), which are 0.97 ± 0.01 eV (1300 °C), 0.93 ± 0.01 eV (1400 °C), 0.97 ± 0.03 eV (1500 °C), 0.80 ± 0.02 eV (1600 °C), 0.93 ± 0.02 eV (1650 °C), and 1.01 ± 0.01 eV (1650 °C-solid), respectively.

The presence of La_2SiO_5 (Fig. 3(c)) has great effect on the grain boundary conduction. As shown in Fig. 7(b), even the sample (prepared by co-precipitation) sintered at 1300 °C exhibits higher grain boundary conductivity than the sample (prepared by solid-

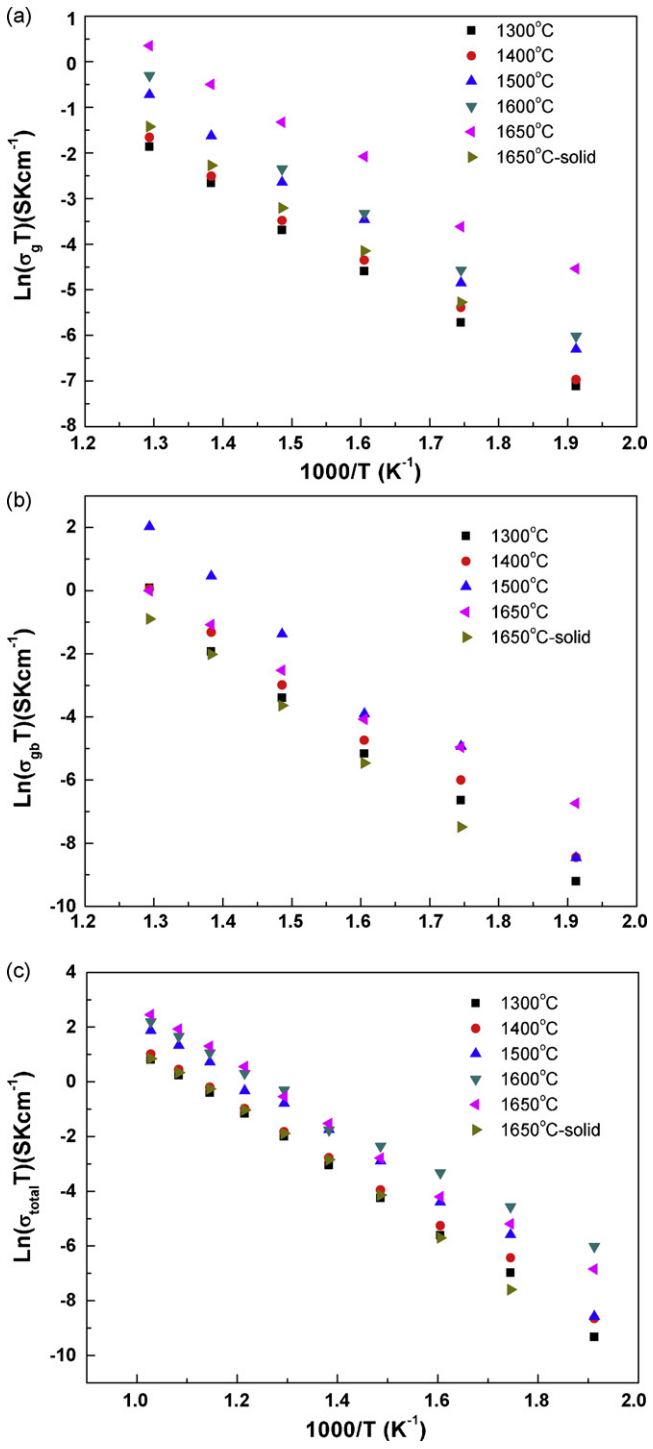

Fig. 7. The grain (a), grain boundary (b) and total (c) conductivities of $La_{10}Si_6O_{27}$ (co-precipitation) sintered at various temperatures. For comparison, the corresponding conductivities of $La_{10}Si_6O_{27}$ (solid-state reaction) sintered at 1650 °C are also shown (1650 °C-solid).

state reaction) sintered at 1650 °C. As is known, higher sintering temperature should correspond to the higher grain conduction due to the homogeneousness of the composition. However, in our work, the sample (prepared by co-precipitation) sintered at 1500 °C shows higher grain conductivity than the sample (prepared by solid-state reaction) sintered at 1650 °C, suggesting the high composition homogeneity for co-precipitation method. Compared to high sintering temperature (1650 °C) for solid-state reaction, co-precipitation methods can effectively reduce the sintering temperature down to 1300 °C with the comparable total conduction value, as shown in Fig. 7(c), due to the absence of the low conductive phase La_2SiO_5. For the best sample (sintered at 1650 °C for 10 h), the conductivity observed is 1.2×10^{-2} S cm^{-1} at 700 °C, which is higher than that of YSZ ceramics [22] and the same composition reported by other investigators [4,5,16].

4. Conclusions

The $La_{10}Si_6O_{27}$ nanopowders with apatite structure were synthesized by co-precipitation method. Pure stoichiometric $La_{10}Si_6O_{27}$ nanopowders were successfully obtained after a 900 °C calcination of precursor powders and then removing La_2O_3 by acid-washing. The ceramics can achieve a high relative density (>95%) at rather low temperature of 1300 °C, which exhibits comparable total conductivity to those sintered at 1650 °C from the powders prepared by conventional methods. Moreover, the sintering temperature has great effect on the electrical conductivity. The enhancement of grain conduction with increasing sintering temperature from 1300 °C to 1650 °C is attributed to the composition homogeneity; while the grain boundary conduction shows the highest value at 1600 °C. For the best value (sintered at 1650 °C for 10 h), the total conductivity observed is 1.2×10^{-2} S cm^{-1} at 700 °C.

Acknowledgment

This research was supported by TOYOTA MOTOR Corp.

References

[1] V.V. Kharton, F.M.B. Marques, A. Atkinson, Solid State Ionics 174 (2004) 135–149.
[2] J.B. Goodenough, Annu. Rev. Mater. Res. 33 (2003) 91–128.
[3] A. Lashtabeg, S.J. Skinner, J. Mater. Chem. 16 (31) (2006) 3161–3170.
[4] S. Nakayama, H. Aono, Y. Sadaoka, Chem. Lett. 6 (1995) 431–432.
[5] S. Nakayama, M. Sakamoto, J. Eur. Ceram. Soc. 18 (10) (1998) 1413–1418.
[6] A. Mineshige, T. Nakao, M. Kobune, T. Yazawa, H. Yoshioka, Solid State Ionics 179 (2008) 1009–1012.
[7] T. Nakao, A. Mineshige, M. Kobune, T. Yazawa, H. Yoshioka, Solid State Ionics 179 (2008) 1567–1569.
[8] E. Kendrick, M. Saiful Islam, P.R. Slater, J. Mater. Chem. 17 (2007) 3104–3111.
[9] R. Ali, M. Yashima, Y. Matsushita, H. Yoshioka, K. Ohoyama, F. Izumi, Chem. Mater. 20 (2008) 5203–5208.
[10] P.R. Slater, J.E.H. Sansom, J.R. Tolchard, Chem. Rec. 4 (2004) 373–384.
[11] H. Yoshioka, J. Am. Ceram. Soc. 90 (10) (2007) 3099–3105.
[12] A.L. Shaula, V.V. Kharton, F.M.B. Marques, J. Solid State Chem. 178 (2005) 2050–2061.
[13] S. Célérier, C. Laberty, F. Ansart, P. Lenormand, P. Stevens, Ceram. Int. 32 (2006) 271–276.
[14] S. Tao, J.T.S. Irvine, Mater. Res. Bull. 36 (2001) 1245–1258.
[15] C. Tian, J. Liu, J. Cai, Y. Zeng, J. Alloys Compd. 458 (2008) 378–382.
[16] A. Chesnaud, G. Dezanneau, C. Estournès, C. Bogicevic, F. Karolak, S. Geiger, G. Geneste, Solid State Ionics 179 (2008) 1929–1939.
[17] A. Chesnaud, C. Bogicevic, F. Karolak, C. Estournès, G. Dezanneau, Chem. Commun. (2007) 1550–1552.
[18] T. Kharlamova, S. Pavlova, V. Sadykov, M. Chaikina, T. Krieger, O. Lapina, D Khabibul, A. Ishchenko, V. Zaikovskii, C. Argirusis, J. Jorge Frade, Eur. J. Inorg. Chem. (2008) 939–947.
[19] E. Rodríguez-Reyna, A.F. Fuentes, M. Maczka, J. Hanuza, K. Boulahya, U. Amador, J. Solid State Chem. 179 (2006) 522–531.
[20] M.I. Mendelson, J. Am. Ceram. Soc. 52 (1969) 443–446.
[21] J.E.H. Sansom, D. Richings, P.R. Slater, Solid State Ionics 139 (2001) 205–210.
[22] N. Takeda, Y. Itagaki, H. Aono, Y. Sadaoka, Sens. Actuator B: Chem. 115 (2006) 455–459.